Spectrochimica Acta Part A 78 (2011) 844–853

Contents lists available at ScienceDirect

Spectrochimica Acta Part A: Molecular and Biomolecular Spectroscopy

journal homepage: www.elsevier.com/locate/saa

Preparation, spectroscopy, EXAFS, electrochemistry and pharmacology of new ruthenium(II) carbonyl complexes containing ferrocenylthiosemicarbazone and triphenylphosphine/arsine

R. Prabhakaran[a,b], S. Anantharaman[c], M. Thilagavathi[a], M.V. Kaveri[a], P. Kalaivani[a], R. Karvembu[d], N. Dharmaraj[a], H. Bertagnolli[c,*], F. Dallemer[b], K. Natarajan[a,**]

[a] Department of Chemistry, Bharathiar University, Coimbatore 641 046, India
[b] Laboratorie Chimie Provence-CNRS UMR6264, University of Aix-Marseille I, II et III – CNRS, Campus Scientifique de Saint-Jérôme, Avenue Escadrille Normandie-Niemen, F-13397 Marseille Cedex 20, France
[c] Institute of Physical Chemistry, University of Stuttgart, Pfaffenwaldring 55, 70569 Stuttgart, Germany
[d] Department of Chemistry, National Institute of Technology, Tiruchirappalli 620 015, India

ARTICLE INFO

Article history:
Received 26 February 2010
Received in revised form
10 December 2010
Accepted 14 December 2010

Keywords:
Ruthenium(II) complexes
Ferrocenylthiosemicarbazone
Spectroscopy
EXAFS
Electrochemistry
Pharmacological studies

ABSTRACT

A new series of new hetero-bimetallic complexes containing iron and ruthenium of the general formula [RuCl(CO)(B)(EPh_3)(L)] (where E = P or As; B = PPh_3, $AsPh_3$, py or pip; L = ferrocene derived monobasic bidentate thiosemicarbazone ligand) have been synthesized by the reaction between ferrocene-derived thiosemicarbazones and ruthenium(II) complexes of the type [RuHCl(CO)(B)(EPh_3)$_2$] (where E = P or As; B = PPh_3, $AsPh_3$, py or pip). The new complexes have been characterized by elemental analyses, IR, electronic, NMR (^{1}H, ^{13}C and ^{31}P), EXAFS (extended X-ray absorption fine structure spectroscopy) and cyclic voltammetric techniques. Antibacterial activity of the new complexes has been screened against *Escherichia coli*, *Vibrio cholerae*, and *Pseudomonas aeruginosa* species.

1. Introduction

Hetero-bimetallic compounds have become increasingly important in recent years in view of their potential applications in the fields of catalysis, drug design [1–3]. Many transition metal complexes of ferrocene derived thiosemicarbazones, semicarbazones are reported [4,5]. Ferrocene and its derivatives have been investigated [6,7] due to their use as colour pigments [8] and as high burning rate catalysts [9]. Even today, cisplatin is one of the most widely used metal containing chemotherapeutic drugs in USA, Europe and Japan [10]. However, it has been shown that certain ferrocenium salts have more favourable 50% lethal dosage (LD_{50}) values compared to cisplatin [11,12]. Moreover, ferrocenylthiosemicarbazone containing transition metal complexes have been found to be active against protozoa [13], tumours [14], pesticides and fungicides [15]. Complexes of thiosemicarbazones have also been screened for medicinal properties [16], shown to possess some degree of cytotoxic activity [17]. In continuation of our interest on bimetallic complexes [18,19], we report in this article, the synthesis, analytical, spectral, characterization, EXAFS studies, antibacterial activities of ferrocenylthiosemicarbazone complexes of ruthenium(II). The general structure of the ligands is given in Fig. 1.

2. Experimental

2.1. Reagents and materials

$RuCl_3 \cdot 3H_2O$ was purchased from Himedia, used without further purification. All the reagents used were chemically pure grade. Solvents were purified, dried according to the standard procedure [20]. Ferrocenylthiosemicarbazone ligands, the starting complexes [RuHCl(CO)(B)(EPh_3)$_2$] (where E = P or As; B = PPh_3, $AsPh_3$, pyridine (py) or pipyridine (pip)) were prepared by the reported procedures [21–25].

* Corresponding author. Tel.: +49 711 685 64450; fax: +49 711 685 64443.
** Corresponding author. Tel.: +91 422 2422222; fax: +91 422 2422387.
E-mail addresses: h.bertagnolli@ipc.uni-stuttgart.de (H. Bertagnolli), k_natraj6@yahoo.com (K. Natarajan).

1386-1425/$ – see front matter © 2010 Elsevier B.V. All rights reserved.
doi:10.1016/j.saa.2010.12.046

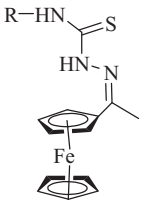

R	Abbreviation
H	HFctsc
C_6H_5	HFcptsc
CH_3	HFcmtsc

Fig. 1. General structure of the ligand.

2.2. Physical measurements

The elemental analyses of the complexes were performed with Vario EL III CHNS analyzer. IR spectra of the ligands and the complexes (KBr pellets) have been recorded with Shimadzu/Nicolet instruments in 4000–400 cm^{-1} range. Electronic spectra of the complexes have been recorded in methanol using a Systronics 119 spectrophotometer in the 800–200 nm range. ^1H NMR, ^{13}C NMR and ^{31}P NMR spectra were recorded in $CDCl_3$ with Varian AMX 400 instrument using tetramethylsilane and orthophosphoric acid as references, respectively. Cyclic voltammetric studies of the complexes have been carried out with EG & G-Princeton Applied Research Electrochemical Analyzer in dichloromethane using a glassy carbon working electrode and all the potentials were referenced to standard silver/silver chloride electrode. Ferrocene was used as external standard. Melting points were recorded on a Raaga melting point apparatus. In spite of several attempts to prepare single crystals, suitable for X-ray structure determination were not succeeded. Hence, the local structure and the coordination geometry of the complexes were determined by extended X-ray absorption fine structure (EXAFS) spectroscopy. The transmission mode EXAFS measurements were performed at Ru K-edge at 22,117 eV, As K-edge at 11,867 eV and Fe K-edge at 7112 eV at the beamline X1.1 of the Hamburger Synchrotron Radiation Laboratory (HASYLAB) at DESY, Hamburg. The complexes were measured with Si(3 1 1) double crystal monochromator at the Ru K-edge, with Si(1 1 1) double crystal monochromator at the As, Fe K-edges. The measurements were carried out at ambient conditions and ion chambers filled with inert gases (nitrogen, argon) were used to measure the incident and transmitted intensities.

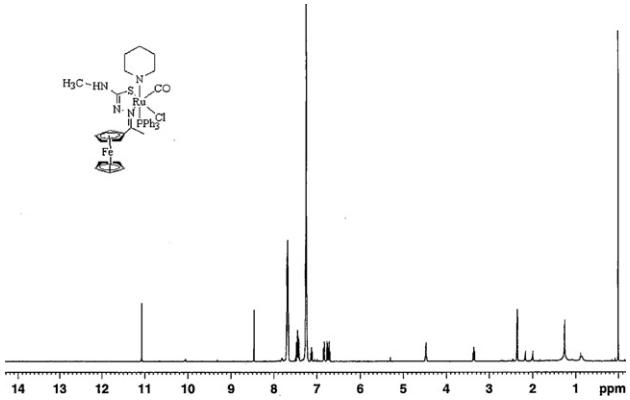

Fig. 2. ^1H NMR spectrum of [RuCl(CO)(pip)(PPh_3)(Fcmtsc)] (**11**).

The positron energy was 4.45 GeV, the beam current was between 90 mA and 130 mA. Energy calibration was monitored by measuring the absorption through a reference simultaneously with the absorption through the complexes, by means of a third ion chamber. For Ru K-edge measurements ruthenium metal foil was used as the reference. A 20-μm thick gold metal foil having L_{III}-edge at 11,919 eV was used as reference for As K-edge measurements. The complexes in solid state were embedded in a polyethylene matrix, pressed into pellet and the concentration was adjusted to yield an extinction of 1.5. Data evaluation started with the removal of background absorption from the experimental absorption spectrum by subtraction of a Victoreen-type polynomial. Then, the spectrum was convoluted with a series of increasingly broader Gaussian functions, the common intersection point of the convoluted spectra was taken as energy E_0 [26,27]. To determine the smooth part of the spectrum, corrected for pre-edge absorption and a piecewise polynomial was used. It was adjusted in such a manner that the low-R components of the resulting Fourier transform were minimal. After division of the background-subtracted spectrum by its smooth part, the photon energy was converted into a photoelectron wave vector scale, the resulting EXAFS function was weighted with k^3. Data analysis in k space was performed according to the curved-wave formalism of the program EXCURVE98 with the XALPHA phase, amplitude functions [28]. The amplitude factor (AFAC) was fixed at 0.8, an overall energy shift (ΔE_0) was introduced to give a best fit to the data. The mean free path of the scattered electrons was calculated from the imaginary part of the potential (VPI was set to −4.00).

2.3. Recommended procedures

2.3.1. Synthesis of new hetero binuclear complexes

To a benzene (25 cm^3) solution of [RuHCl(CO)(PPh_3)$_3$] (0.030 g; 0.1 mmol) and the ferrocenylthiosemicarbazone ligand (HFctsc) (0.095 g; 0.1 mmol) was added. The mixture was refluxed for 6 h and the resulting brown solution was concentrated to about 3 cm^3. The new complex was separated by adding a small quantity (6 cm^3) of petroleum ether (60–80 °C). They were recrystallised from CH_2Cl_2/petroleum ether (60–80 °C) mixture and dried *in vacuo*. *[RuCl(CO)(PPh_3)$_2$(Fctsc)]* (**1**) yield: 70% (66.7 mg). M.p. > 300 °C. FT-IR (KBr): 1625 cm^{-1} ($\nu_{C=N}$), 1957 cm^{-1} ($\nu_{C\equiv O}$), 748 cm^{-1} (ν_{C-S}), 1433, 1093, and 693 cm^{-1} (for PPh_3). UV–vis (methanol), λ_{max} (234, 260, 281, 302, and 466 nm). Anal. Calc. for $C_{50}H_{44}N_3OP_2SClFeRu$: C, 60.7; H, 4.48; N, 4.25; S, 3.24; Found: C, 59.98; H, 5.18; N, 4.97; S, 4.02. ^1H NMR ($CDCl_3$ δ ppm); 7.0–7.9 (m, aromatic), 2.2 (s, CH_3), 4.2 (s, Cp ring), 5.4 (s, $-NH_2$); ^{31}P NMR ($CDCl_3$ δ ppm); 28.6.

The similar procedure has been followed to prepare the other complexes also.

[RuCl(CO)(PPh_3)(py)(Fctsc)] (**2**) yield: 65% (50.09 mg). M.p. > 300 °C. FT-IR (KBr): 1620 cm^{-1} ($\nu_{C=N}$), 1948 cm^{-1} ($\nu_{C\equiv O}$), 755 cm^{-1} (ν_{C-S}), 1436, 1070, and 694 cm^{-1} (for PPh_3). UV–vis (methanol), λ_{max} (232, 255, 290, and 476 nm). Anal. Calc. for $C_{37}H_{34}N_4OPSClFeRu$: C, 55.13; H, 4.25; N, 6.95; S, 3.98; Found: C, 55.89; H, 4.72; N, 6.44; S, 4.04. ^1H NMR ($CDCl_3$ δ ppm); 6.9–7.7 (m, aromatic), 2.25 (s, CH_3), 4.1 (s, Cp ring), 5.4 (s, $-NH_2$).

[RuCl(CO)(PPh_3)(pip)(Fctsc)] (**3**) yield: 55% (42.72 mg). M.p. > 300 °C. FT-IR (KBr): 1618 cm^{-1} ($\nu_{C=N}$), 1944 cm^{-1} ($\nu_{C\equiv O}$), 746 cm^{-1} (ν_{C-S}), 1434, 1093, and 696 cm^{-1} (for PPh_3). UV–vis (methanol), λ_{max} (221, 260, 294, 442, and 468 nm). Anal. Calc. for $C_{37}H_{39}N_4OPSClFeRu$: C, 54.78; H, 4.85; N, 6.9; S, 3.95; Found: C, 55.08; H, 4.48; N, 3.90; S, 3.08.

[RuCl(CO)($AsPh_3$)$_2$(Fctsc)] (**4**) yield: 65% (67.71 mg). M.p. 258 °C. FT-IR (KBr): 1618 cm^{-1} ($\nu_{C=N}$), 1956 cm^{-1} ($\nu_{C\equiv O}$), 736 cm^{-1} (ν_{C-S}), 1438, 1088, and 704 cm^{-1} (for $AsPh_3$). UV–vis (methanol), λ_{max} (267, 293, 327, 368, and 464 nm). Anal. Calc. for

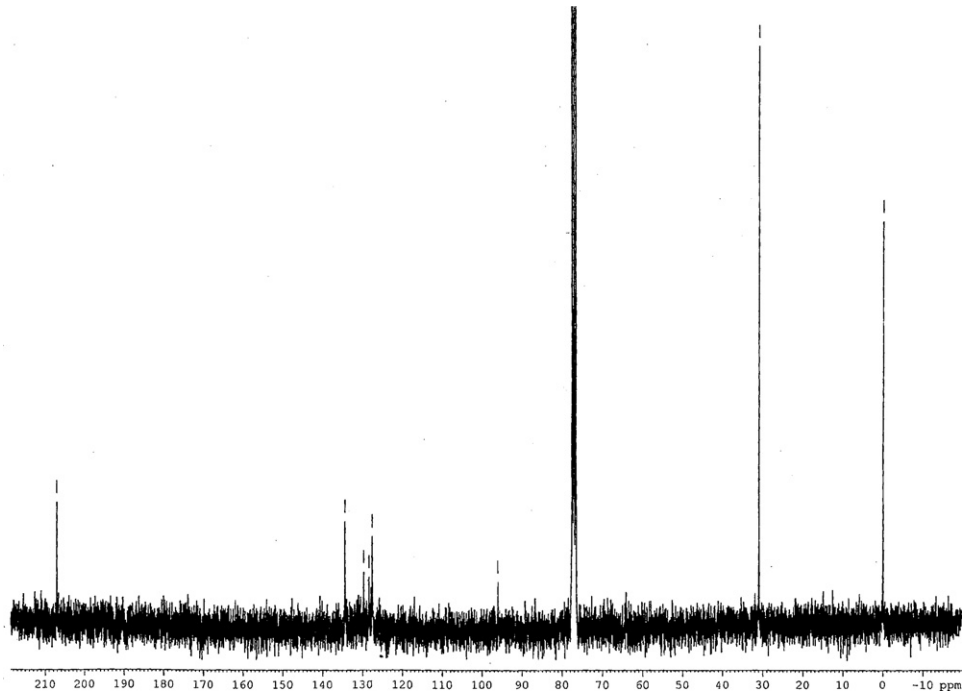

Fig. 3. ^{13}C NMR spectrum of [RuCl(CO)(PPh_3)$_2$(Fcptsc)] (**5**).

$C_{50}H_{44}N_3OAs_2SClFeRu$: C, 55.75; H, 4.10; N, 3.90; S, 2.97; Found: C, 56.08; H, 4.48; N, 4.28; S, 3.08.

[RuCl(CO)(PPh_3)$_2$(Fcptsc)] (**5**) yield: 65% (66.95 mg). M.p. > 300 °C. FT-IR (KBr): 1600 cm^{-1} ($\nu_{C=N}$), 1935 cm^{-1} ($\nu_{C\equiv O}$), 744 cm^{-1} (ν_{C-S}), 1435, 1095, and 698 cm^{-1} (for PPh_3). UV–vis (methanol), λ_{max} (264, 298, 324, 370, and 468 nm). Anal. Calc. for $C_{56}H_{48}N_3OP_2SClFeRu$: C, 65.30; H, 4.69; N, 4.07; S, 3.11; Found: C, 64.93; H, 4.88; N, 3.98; S, 3.25. ^1H NMR ($CDCl_3$ δ ppm); 6.5–8.1 (m, aromatic), 1.98 (s, CH_3), 4.2 (s, Cp ring), 11.8 (s, terminal –NH), ^{13}C NMR ($CDCl_3$ δ ppm); 207 (CO), 134.4, 129.7, 128.4, 127.6 (phenyl protons), 96 (cyclo pentadienyl), 30.9 (CH_3); ^{31}P NMR ($CDCl_3$ δ ppm); 36.25.

[RuCl(CO)(PPh_3)(py)(Fcptsc)] (**6**) yield: 65% (55.04 mg). M.p. > 300 °C. FT-IR (KBr): 1602 cm^{-1} ($\nu_{C=N}$), 1965 cm^{-1} ($\nu_{C\equiv O}$), 742 cm^{-1} (ν_{C-S}), 1434, 1092, and 698 cm^{-1} (for PPh_3). UV–vis (methanol), λ_{max} (242, 292, 360, and 465 nm). Anal. Calc. for $C_{43}H_{38}N_4OPSClFeRu$: C, 60.99; H, 4.52; N, 6.61; S, 3.78; Found: C, 60.16; H, 4.48; N, 6.88; S, 4.08. ^1H NMR ($CDCl_3$ δ ppm); 6.2–7.4 (m, aromatic), 1.7 (s, CH_3), 4.1 (s, Cp ring), 11.6 (s, terminal –NH).

[RuCl(CO)(PPh_3)(pip)(Fcptsc)] (**7**) yield: 60% (51.17 mg). M.p. > 300 °C. FT-IR (KBr): 1600 cm^{-1} ($\nu_{C=N}$), 1930 cm^{-1} ($\nu_{C\equiv O}$), 746 cm^{-1} (ν_{C-S}), 1431, 1086, and 704 cm^{-1} (for PPh_3). UV–vis (methanol), λ_{max} (228, 296, 326, 370, and 471 nm). Anal. Calc. for $C_{43}H_{43}N_4OPSClFeRu$: C, 60.56; H, 5.20; N, 6.56; S, 3.76; Found: C, 61.48; H, 5.36; N, 7.08; S, 3.96. ^1H NMR ($CDCl_3$ δ ppm); 6.0–7.8 (m, aromatic), 2.1 (s, CH_3), 4.15 (s, Cp ring), 3.1–3.5 (m, pip), 11.6 (s, terminal –NH).

[RuCl(CO)($AsPh_3$)$_2$(Fcptsc)] (**8**) yield: 75% (83.84 mg). M.p. > 300 °C. FT-IR (KBr): 1602 cm^{-1} ($\nu_{C=N}$), 1957 cm^{-1} ($\nu_{C\equiv O}$), 748 cm^{-1} (ν_{C-S}), 1436, 1092, and 696 cm^{-1} (for $AsPh_3$). UV–vis (methanol), λ_{max} (223, 260, 277, 320, and 460 nm). Anal. Calc. for $C_{56}H_{48}N_3OAs_2SClFeRu$: C, 60.17; H, 4.32 N, 3.75; S, 2.87; Found: C,

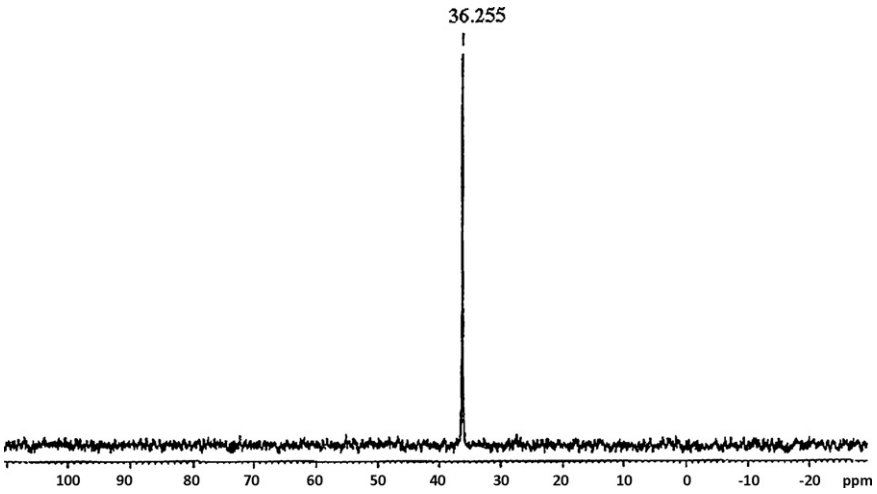

Fig. 4. ^{31}P NMR spectrum of [RuCl(CO)(PPh_3)$_2$(Fcptsc)] (**5**).

59.86; H, 4.62; N, 4.16; S, 3.02. ^{1}H NMR ($CDCl_3$ δ ppm); 6.5–7.8 (m, aromatic), 1.63 (s, CH_3), 4.2 (s, Cp ring), 11.6 (s, terminal –NH).

[RuCl(CO)(PPh$_3$)$_2$(Fcmtsc)] (**9**) yield: 65% (62.91 mg). M.p. > 300 °C. FT-IR (KBr): 1640 cm^{-1} ($\nu_{C=N}$), 1951 cm^{-1} ($\nu_{C\equiv O}$), 748 cm^{-1} (ν_{C-S}), 1434, 1094, and 695 cm^{-1} (for PPh_3). UV–vis (methanol), λ_{max} (234, 260, 281, 302, and 466 nm). Anal. Calc. for $C_{51}H_{46}N_3OP_2SClFeRu$: C, 61.05; H, 4.60; N, 4.19; S, 3.20; Found: C, 60.21; H, 4.74; N, 4.19; S, 3.24.

[RuCl(CO)(PPh$_3$)(py)(Fcmtsc)] (**10**) yield: 65% (51 mg). M.p. > 300 °C. FT-IR (KBr): 1647 cm^{-1} ($\nu_{C=N}$), 1953 cm^{-1} ($\nu_{C\equiv O}$), 748 cm^{-1} (ν_{C-S}), 1431, 1095, and 696 cm^{-1} (for PPh_3). UV–vis (methanol), λ_{max} (230, 260, 298, and 466 nm). Anal. Calc. for $C_{38}H_{36}N_4OPSClFeRu$: C, 55.65; H, 4.42; N, 6.83; S, 3.91; Found: C, 56.04; H, 4.68; N, 7.04; S, 4.16.

[RuCl(CO)(PPh$_3$)(pip)(Fcmtsc)] (**11**) yield: 60% (47.44 mg). M.p. > 300 °C. FT-IR (KBr): 1647 cm^{-1} ($\nu_{C=N}$), 1951 cm^{-1} ($\nu_{C\equiv O}$), 748 cm^{-1} (ν_{C-S}), 1434, 1093, and 692 cm^{-1} (for PPh_3). UV–vis (methanol), λ_{max} (238, 272, 296, 346, and 462 nm). Anal. Calc. for $C_{38}H_{41}N_4OPSClFeRu$: C, 55.31; H, 5.00; N, 6.79; S, 3.89; Found: C, 54.98; H, 4.98; N, 7.03; S, 4.01. ^{1}H NMR ($CDCl_3$ δ ppm); 6.7–7.8 (m, aromatic), 2.2 (s, CH_3), 4.4 (m, Cp ring), 3.2–3.5 (m, pip), 2.4 (m, NH–CH_3), 11.8 (s, terminal –NH).

[RuCl(CO)(AsPh$_3$)$_2$(Fcmtsc)] (**12**) yield: 75% (79.18 mg). M.p. > 300 °C. FT-IR (KBr): 1631 cm^{-1} ($\nu_{C=N}$), 1955 cm^{-1} ($\nu_{C\equiv O}$), 740 cm^{-1} (ν_{C-S}), 1438, 1094, and 702 cm^{-1} (for $AsPh_3$). UV–vis (methanol), λ_{max} (242, 302, 350, 385, and 474 nm). Anal. Calc. for $C_{51}H_{46}N_3OAs_2SClFeRu$: C, 56.14; H, 4.25; N, 3.85; S, 2.94; Found: C, 56.28; H, 4.37; N, 3.98; S, 3.18.

2.3.2. Procedure for antibacterial activity studies

Antibacterial activity of the ligands and ruthenium(II) complexes have been carried out against the pathogenic bacteria *Escherichia coli*, *Vibrio cholerae* and *Pseudomonas aeruginosa* species [29]. The test organisms were grown on nutrient agar medium in Petri plates. The complexes to be tested were dissolved in $CHCl_3$ and soaked in filter paper disc of 5 mm diameter and 1 mm thickness. The concentrations used in this study were 0.25–2%. The discs were placed on the previously seeded plates and incubated at 37 °C for 24 h. The diameter (mm) of the inhibition zone around each disc was measured after 24 h. *Streptomycin* was used as standard.

3. Results and discussion

The new ruthenium(II) complexes are stable to air, light stable and soluble in organic solvents such as benzene, $CHCl_3$, CH_2Cl_2, DMF and DMSO. The elemental analyses obtained for the complexes are in good agreement with the proposed molecular formula. In all the reactions, it has been observed that the ferrocenylthiosemicarbazones behaved as monofunctional bidentate ligand by substituting one of the triphenylphosphines / triphenylarsines and a hydride ion from the starting complexes (Scheme 1). One interesting aspect is that the heterocyclic nitrogen base (pyridine or piperidine) remains intact without being eliminated in the complexes. The reason for the non-replacement of coordinated bases is due to the fact that the Ru–P or Ru–As bond is more labile than Ru–N bond due to the better σ-donating ability of nitrogen atom [30].

3.1. IR spectra

The IR spectra of the complexes have been compared with that of the ligands in order to fix the mode of coordination. The free ligands showed a very strong absorption around 1651–1654 cm^{-1} characteristic of the azomethine (>C=N) group. In all the complexes, the band due to azomethine was observed at a lower region around 1600–1647 cm^{-1} indicating the coordination of azomethine nitrogen to ruthenium [30]. In the IR spectra of all the new complexes, a strong band in the region 1930–1965 cm^{-1} has been observed due to the presence of terminally coordinated carbonyl group [28]. A medium intensity band observed in the region 821–823 cm^{-1} in the spectra of the ligands has been assigned as due to >C=S, which was completely disappeared in the complexes and a new band appeared in the region 736–755 cm^{-1} indicating coordination of thiolate sulphur after the enolisation of –NH–C=S– group and subsequent deprotonation [31,32]. Characteristic bands due to triphenylphosphine / triphenylarsine were also present in the expected region. The complexes containing coordinated nitrogen bases exhibited a medium intensity band around 1020–1040 cm^{-1} region, which is characteristic of coordinated pyridine or piperidine [30].

3.2. Electronic spectra

All the new ruthenium(II) complexes have been found to be diamagnetic indicating the presence of ruthenium in +2 oxidation state. The ground state of ruthenium(II) (t_{2g}^6 configuration) is $^1A_{1g}$. The excited states corresponding to t_{2g}^5 e_g^1 configuration are $^3T_{1g}$, $^3T_{2g}$, $^1T_{1g}$ and $^1T_{2g}$ in the order of increasing energy. Hence, four bands are possible corresponding to the transitions $^1A_{1g} \rightarrow {}^3T_{1g}$, $^1A_{1g} \rightarrow {}^3T_{2g}$, $^1A_{1g} \rightarrow {}^1T_{1g}$ and $^1A_{1g} \rightarrow {}^1T_{2g}$, in the order of increasing energy. The electronic spectra of all the complexes were recorded in methanol. The spectra of the complexes showed four to five bands in the region 221–476 nm. The bands appearing in the region 330–385 nm have been assigned to charge transfer transitions arising from excitation of an electron from the metal t_{2g} level to an unfilled molecular orbital derived form the π^* level of the ligands [33]. This assignment is in conformity with the assignments made for similar other ruthenium(II) octahedral complexes [34]. The broad band observed around 442–476 nm in the complexes may be assigned to charge transfer from the iron to either the non-bonding or anti-bonding orbitals of the cyclopentadienyl ring [35].

3.3. NMR spectra

^{1}H NMR spectra of some of the complexes have been recorded to confirm the presence of the coordinated ferrocenylthiosemicarbazone ligands. In all the complexes, a broad multiplet observed in the region 6.5–8.1 ppm is due to the aromatic protons of the phenyl groups in triphenylphosphine / triphenylarsine and thiosemicarbazone ligand [29]. The sharp singlets/multiplets observed around 4.1–4.4 ppm and 1.58–2.2 ppm was assigned to the protons of ferrocenyl cyclopentadienyl ring and methyl groups, respectively [36] (Fig. 2). A broad multiplet appeared around 3.1–3.5 ppm for the complexes **7** and **11** is due to the protons of piperidine. In the spectra of the complexes **5**, **6**, **7**, **8** and **11**, a singlet is observed at 11.6–11.8 ppm due to the –NH– proton of ligand [37]. There is an another multiplet at 2.4 ppm was observed for terminal CH_3 group of the coordinated ligand [31]. The complexes **1** and **2** showed a sharp singlet at 5.4 ppm due to $-NH_2-$ protons [21]. A representative ^{13}C NMR spectrum of the complex **5** was recorded and it contains four signals corresponding to the aromatic protons at 134.4, 129.7, 128.4, and 127.6 ppm of triphenylphosphine and phenyl group of the ligand (Fig. 3). A carbonyl carbon signal appears at 207 ppm and the signals corresponding to cyclo pentadienyl carbons also found at 96 ppm. In addition, a signal corresponding to methyl group of the ligand was found at 30.9 ppm. In order to confirm the presence of triphenylphosphine group and determine the geometry of the ruthenium(II) complexes, a representative ^{31}P NMR spectra were recorded for complexes **1** and **5**. A singlet

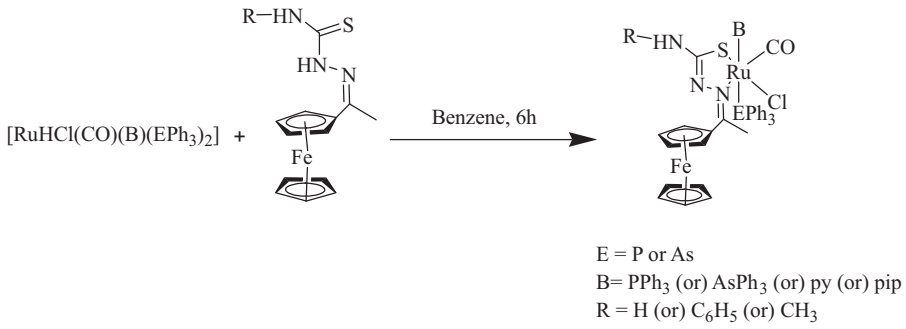

Scheme 1. Preparation of new hetero-bimetallic binuclear complexes.

observed at 28.6 ppm and 36.25 ppm suggested the presence of two magnetically equivalent triphenylphosphine groups *trans* to each other (Fig. 4) [38].

3.4. Electrochemistry

Typical cyclic voltammogram of new hetero-bimetallic mixed valance complexes in dichloromethane showed a pair of peaks on both positive and negative potential sides, corresponding to two successive one electron oxidation Fe^{II}–$Ru^{II} \rightarrow Fe^{III}$–$Ru^{II} \rightarrow Fe^{III}$–$Ru^{III}$ and similar one electron reduction Fe^{II}–$Ru^{II} \rightarrow Fe^{I}$–$Ru^{II} \rightarrow Fe^{I}$–$Ru^{I}$ processes. The observed oxidation potential values of Fe^{II}–$Ru^{II} \rightarrow Fe^{III}$–$Ru^{III}$ were found to be in good agreement with the reported values for Fe(II)–Fe(III) and Ru(II)–Ru(III) process. The comproportionation constant values for these complexes indicate a strong electronic coupling between iron and ruthenium ions (Table 1) and confirm the strong coupling is through –Cp–C=N–N=C–S– spacer. We strongly feel that this is one of the better examples of class-III type of hetero binuclear complex with long range coupling [39]. The comproportionation values for the reduction processes were higher than that of the oxidation process in the complexes **4**, **5**, **8**, **10**, **11** and **12** which is a strong evidence for the existence of Fe(I)–Ru(I) oxidation states (Fig. 5). It reveals that the electronic coupling between Fe(I) and Ru(I) is as strong as Fe(III)–Ru(III) coupling. The equilibrium constant K_c for comproportionation reaction in these hetero-bimetallic mixed valence complexes is defined as:

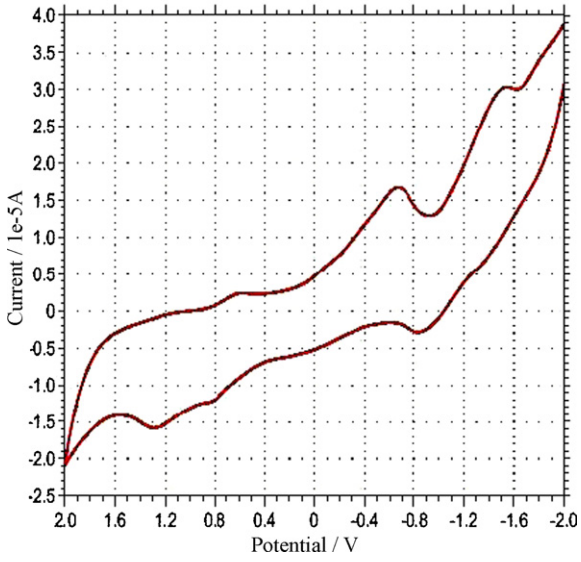

Fig. 5. Cyclic voltammogram of [RuCl(CO)($AsPh_3$)$_2$(Fcmtsc)] (**12**).

Oxidation

$$Fe(II)\text{–}Ru(II) \underset{E_{1/2}(\text{Oxd 1})}{\overset{-e^-}{\rightleftharpoons}} Fe(III)\text{–}Ru(II) \underset{E_{1/2}(\text{Oxd 2})}{\overset{-e^-}{\rightleftharpoons}} Fe(III)\text{–}Ru(III)$$

Reduction

$$Fe(II)\text{–}Ru(II) \underset{E_{1/2}(\text{Red 1})}{\overset{e^-}{\rightleftharpoons}} Fe(I)\text{–}Ru(II) \underset{E_{1/2}(\text{Red 2})}{\overset{e^-}{\rightleftharpoons}} Fe(I)\text{–}Ru(I)$$

$$K_c(\text{II–III}) = \frac{[Fe(III)\text{–}Ru(II)]^2}{[Fe(II)\text{–}Ru(II)][Fe(III)\text{–}Ru(III)]}$$

$$K_c(\text{II–I}) = \frac{[Fe(I)\text{–}Ru(II)]^2}{[Fe(II)\text{–}Ru(II)][Fe(I)\text{–}Ru(I)]}$$

$$K_c = \exp^{(F/RT)[E_{1/2}(1)-E_{1/2}(2)]}$$

3.5. EXAFS studies

EXAFS spectroscopy provides information on the coordination number, the nature of the scattering atoms surrounding the absorbing atom, the interatomic distance between the absorbing atom and the backscattering atoms and the Debye–Waller factor which accounts for the disorders due to the static displacements and thermal vibrations. In the fitting procedure, for all the cases the coordination numbers were fixed to known values for different backscatterers surrounding the excited atom, and the other parameters including interatomic distances, Debye–Waller factor and Fermi energy value were varied by interactions.

3.5.1. Fe K-edge investigation

The experimentally determined and theoretically calculated EXAFS functions in k space and their Fourier transforms in real space for the different ruthenium(II) ferrocenylthiosemicarbazone complexes containing triphenylphosphine/arsine were measured. In order to study the presence of ferrocenyl unit, the measurement was done at Fe K-edge are shown in Fig. 6a–c and the corresponding structural parameters are summarized in Table 2. In the analysis of the complexes **1**, **4** and **5** the shell was determined at about 1.99–2.07 Å corresponding to Fe–C backscatterers arising from the ferrocenyl unit. This value is in good agreement with the reported value [40]. The EXAFS results indicate the attachment of ten carbon atoms of both the cyclopentadienyl ligand to Fe centre.

3.5.2. Ru K-edge investigation

EXAFS evaluations were performed at k space were measured at the Ru K-edge are shown in Fig. 7a–c and the corresponding structural parameters are summarized in Table 3. In the analysis of the complexes **1**, **4** and **5**, the first shell was determined at about

Table 1
Electrochemical data of Fe(II)–Ru(II) complexes.

Complex	Reduction (V)				Oxidation (V)			
	$E_{1/2}(1)$	$E_{1/2}(2)$	$\log K_c$	K_c	$E_{1/2}(1)$	$E_{1/2}(2)$	$\mathrm{Log}\,K_c$	K_c
(2)	0.347	–	–	–	1.092	0.577	8.71	5.13×10^{8}
(4)	0.778	−0.449	20.75	5.6×10^{20}	1.462	0.568	15.12	1.32×10^{15}
(5)	0.576	−0.589	19.7035	5.1×10^{19}	1.066	0.378	11.63	4.23×10^{11}
(6)	0.984	–	–	–	1.460	0.837	10.54	3.44×10^{10}
(8)	0.70	−0.212	15.425	2.6×10^{15}	1.246	0.462	13.26	1.82×10^{13}
(9)	0.363	−0.274	10.77	6.0×10^{10}	.939	0.081	14.51	3.24×10^{4}
(10)	0.337	−0.724	17.95	2.8×10^{17}	1.056	0.316	12.515	3.3×10^{12}
(11)	0.338	−0.772	18.733	5.9×10^{18}	1.241	0.585	11.09	1.25×10^{11}
(12)	0.364	0.562	15.66	4.5×10^{15}	1.254	0.808	7.54	3.49×10^{7}

Fe K-edge (7112 eV) measurements

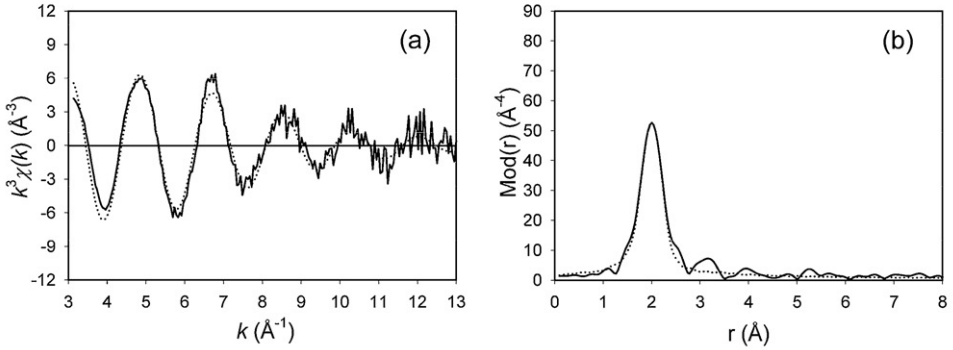

a Experimental (solid line) and calculated (dotted line) EXAFS function and Fourier Transform plots for [RuCl(CO)(PPh$_3$)$_2$(Fctsc)] (1)measured at the Fe K-edge.

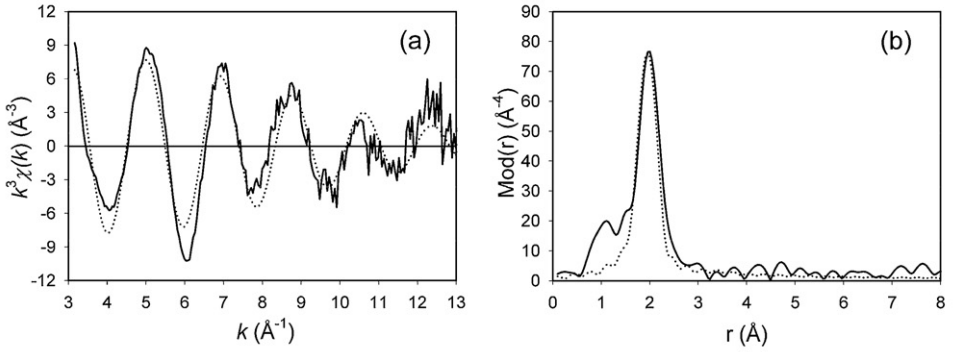

b Experimental (solid line) and calculated (dotted line) EXAFS function and Fourier Transform plots for [RuCl(CO)(AsPh$_3$)$_2$(Fctsc)](4)measured at the Fe K-edge.

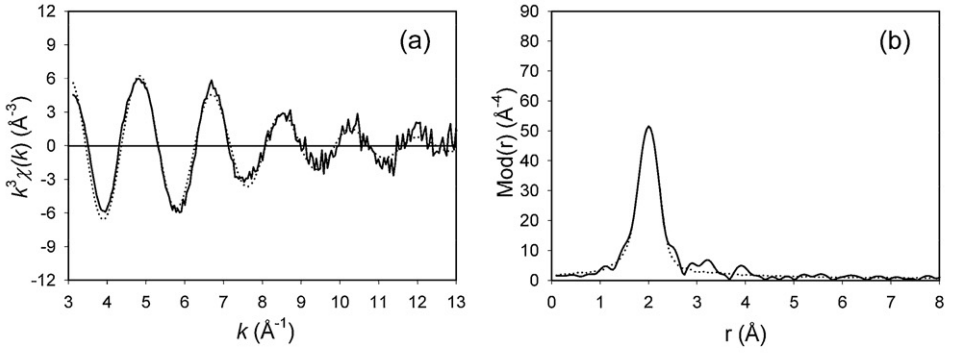

c Experimental (solid line) and calculated (dotted line) EXAFS function and Fourier Transform plots for [RuCl(CO)(PPh$_3$)$_2$(Fcptsc)] (5) measured at the Fe K-edge.

Fig. 6. Experimental (solid line) and calculated (dotted line) EXAFS function and Fourier Transform plots for (a) [RuCl(CO)(PPh$_3$)$_2$(Fctsc)] (**1**), (b) [RuCl(CO)(AsPh$_3$)$_2$(Fctsc)] (**4**), and (c) [RuCl(CO)(PPh$_3$)$_2$(Fcptsc)] (**5**), measured at the Fe K-edge (7112 eV).

Table 2
EXAFS determined structural parameters at Fe K-edge.

Complex	A–Bs[a]	N[b]	r[c] [Å]	σ[d] [Å]	E_F[e] [eV]	k-range [Å^{-1}]	R-factor
1	Fe–C	10	2.04 ± 0.02	0.095 ± 0.009	7.522	3.13–3.04	31.94
4	Fe–C	10	2.01 ± 0.02	0.084 ± 0.008	8.943	3.13–3.01	30.76
5	Fe–C	10	2.07 ± 0.02	0.092 ± 0.009	5.841	3.06–3.03	36.37

[a] Absorber (A) – backscatterers (Bs).
[b] Coordination number N.
[c] Interatomic distance r.
[d] Debye–Waller factor σ with its calculated deviation.
[e] Fermi energy E_F.

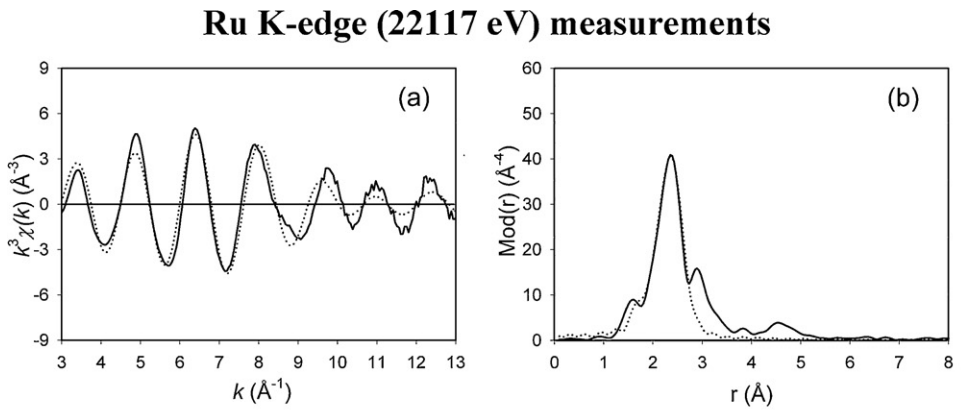

a Experimental (solid line) and calculated (dotted line) EXAFS function and Fourier Transform plots for [RuCl(CO)(PPh$_3$)$_2$(Fctsc)] (1) measured at the Ru K-edge.

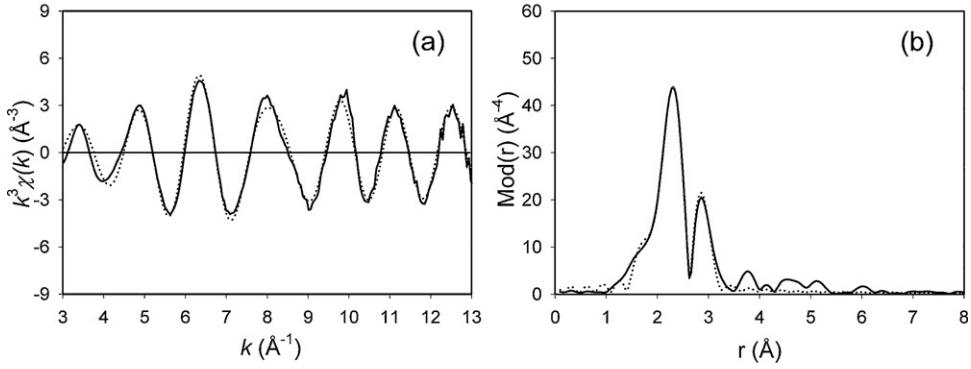

b Experimental (solid line) and calculated (dotted line) EXAFS function and Fourier Transform plots for [RuCl(CO)(AsPh$_3$)$_2$(Fctsc)] (4) measured at the Ru K-edge.

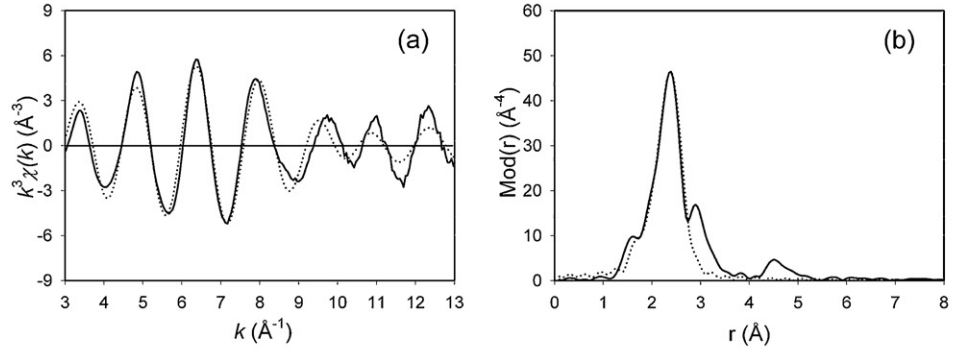

c Experimental (solid line) and calculated (dotted line) EXAFS function and Fourier Transform plots for [RuCl(CO)(PPh$_3$)$_2$(Fcptsc)] (5) measured at the Ru K-edge.

Fig. 7. Experimental (solid line) and calculated (dotted line) EXAFS function and Fourier Transform plots for (a) [RuCl(CO)(PPh$_3$)$_2$(Fctsc)] (**1**), (b) [RuCl(CO)(AsPh$_3$)$_2$(Fctsc)] (**4**), and (c) [RuCl(CO)(PPh$_3$)$_2$(Fcptsc)] (**5**), measured at the Ru K-edge (22117 eV).

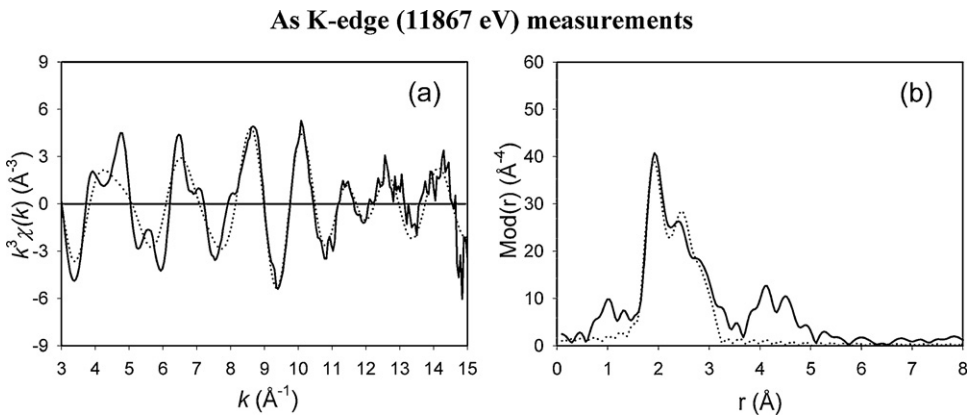

Fig. 8. Experimental (solid line) and calculated (dotted line) EXAFS function and Fourier Transform plots for [RuCl(CO)($AsPh_3$)$_2$(Fctsc)](**4**) measured at the As K-edge (11867 eV).

1.85 Å with one carbon backscatterer arising from the coordinated CO ligand.

This value is in very good agreement with the value of 1.86 Å reported for ruthenium carbonyl clusters [41]. The second shell was determined at about 2.25 Å, it was fitted with a coordination number of one consisting of a nitrogen backscatterer in [RuCl(CO)(PPh_3)$_2$(Fctsc)](**1**) and in the complexes **1**, **4** and **5** were fitted with a coordination number of one consisting of a nitrogen backscatterer from the corresponding ligand, in the case of the [RuCl(CO)(PPh_3)$_2$(Fctsc)](**1**) and [RuCl(CO)($AsPh_3$)$_2$ (Fctsc)](**4**). For the complex [RuCl(CO)(PPh_3)$_2$(Fcptsc)](**5**), it was fitted at about 2.20 Å, similar to backscattering behaviour of the near neighbours (chlorine, sulphur and two phosphorous backscatterers) occurring at nearly the same distance. Hence, they could not be fitted separately in the complexes **1** and **5** and thus were fitted into the single shell with combined coordination number with sulphur amplitude and phase functions. Whereas in the complex **4**, the second shell was determined at about 2.44 Å consisting of one sulphur and one chlorine backscatterers. This is because of the similar backscattering behaviour of the near neighbour (sulphur and chlorine) occurring at nearly the same distance and hence they could not be fitted separately, thus were fitted as one shell with sulphur amplitude and phase functions. In addition, two arsenic backscatterers were determined at about 2.45 Å distance. The determined Ru–As distance was in good agreement with those reported for similar ruthenium complexes [42–44]. The determined Ru–N, Ru–C and Ru–P/Cl/S distances are in good agreement with the reported complexes.

3.5.3. As K-edge investigation

The EXAFS evaluation at the As K-edge was performed using the multiple scattering formalism, as there could be considerable interference effects due to the neighbouring backscatterers. The multiple scattering calculations were done considering all the different pathways surroundings the central arsenic atom. The maximum order of scattering and the maximum atoms in one path were set to three and the maximum path length was set to ten during the calculations. The experimentally determined and theoretically calculated EXAFS functions in k space and their Fourier transforms in real space for the different ruthenium(II)ferrocenylthiosemicarbazone complexes with triphenylarsine measured at the As K-edge evaluated using the multiple scattering formalism are shown in Fig. 8. The EXAFS determined structural parameters are given in Table 4. In the complex **(4)**, the k^3-weighted EXAFS function was best described by a three-shell model. The first shell at about 1.95 Å was fitted with the carbon backscatterers originating from the proximal carbon atoms of the coordinating triphenylarsine group. The reported arsenic–carbon distances ranges from 1.90 Å to 1.97 Å. The second shell consisting of a single ruthenium backscatterer was determined at about 2.45 Å and the third shell comprising of six carbon backscatterers stemming from the second near-neighbour carbon atoms of the phenyl ring was determined [45].

On the basis of IR, electronic, NMR spectral data and EXAFS, an octahedral geometry has been confirmed for the new hetero-bimetallic complexes (Fig. 9).

Table 3
EXAFS determined structural parameters at the Ru K-edge.

Complex	A–Bs[a]	N[b]	r[c] [Å]	σ[d] [Å]	E_F[e] [eV]	k-range [Å^{-1}]	R-factor
	Ru–C	1	1.85 ± 0.02	0.055 ± 0.006			
1	Ru–N	1	2.25 ± 0.02	0.063 ± 0.009	2.692	2.94–13.07	34.73
	Ru–S/P/Cl	4	2.41 ± 0.02	0.102 ± 0.015			
4	Ru–C	1	1.84 ± 0.02	0.050 ± 0.005			
	Ru–N	1	2.24 ± 0.02	0.105 ± 0.015	2.966	3.11–13.04	21.75
	Ru–S/Cl	2	2.39 ± 0.02	0.055 ± 0.008			
	Ru – As	2	2.75 ± 0.02	0.100 ± 0.015			
5	Ru – C	1	1.85 ± 0.02	0.050 ± 0.005			
	Ru – N	1	2.20 ± 0.02	0.112 ± 0.017	1.755	2.96–13.02	33.61
	Ru – S/P/Cl	4	2.42 ± 0.02	0.095 ± 0.014			

[a] Absorber (A) – backscatterers (Bs).
[b] Coordination number N.
[c] Interatomic distance r.
[d] Debye–Waller factor σ with its calculated deviation.
[e] Fermi energy E_F.

Table 4
EXAFS determined structural parameters at the As K-edge.

Complex	A–Bs[a]	N[b]	r[c] [Å]	σ[d] [Å]	E_F[e] [eV]	k-range [Å^{-1}]	R-factor
4	As–C	3	1.95 ± 0.02	0.050 ± 0.005	−3.637	2.92–15.04	41.58
	As–Ru	1	2.45 ± 0.02	0.071 ± 0.010			
	As–C	6	2.92 ± 0.03	0.084 ± 0.012			

[a] Absorber (A) – backscatterers (Bs).
[b] Coordination number N.
[c] Interatomic distance r.
[d] Debye–Waller factor σ with its calculated deviation.
[e] Fermi energy E_F.

Table 5
Antibacterial activity of ruthenium(II) Schiff base complexes.

Compound	Diameters inhibition zone (mm)											
	E. coli				*Vibrio cholerae*				*P. aeruginosa*			
	0.25	0.5	1	2	0.25	0.5	1	2	0.25	0.5	1	2
HFctsc	5	7	8	–	4	6	8	9	–	5	7	9
HFcptsc	4	6	8	9	5	6	7	9	6	8	–	9
HFcmtsc	5	5	7	8	–	–	6	8	7	7	8	9
(**2**)	–	–	–	–	12	13	13	14	11	11	12	13
(**3**)	10	12	12	14	11	12	15	16	12	13	14	–
(**4**)	–	–	–	–	11	12	12	13	–	10	12	13
(**5**)	12	14	15	17	13	15	16	–	10	12	13	16
(**6**)	–	15	16	18	11	13	–	18	–	13	14	–
(**7**)	12	14	15	17	–	12	13	15	–	–	15	17
(**8**)	11	13	15	16	11	13	14	16	11	12	14	–
(**9**)	–	–	–	–	10	11	–	–	11	11	12	15
(**10**)	10	11	–	–	–	–	–	–	11	12	13	14
(**12**)	11	11	12	13	10	12	13	14	10	11	–	14
Streptomycin	18	20	22	25	14	17	20	22	18	21	23	24

3.6. Antibacterial activity

Antibacterial activity of the ligands and the complexes has been carried out against *E. coli*, *V. cholerae* and *P. aeruginosa*, the results were given in Table 5. From the data we observed that the metal chelates exhibited higher activity than the respective free ligands. Such increased activity of the metal chelates can be explained on the basis of Overtone's concept and chelation theory [46]. According to Overtone's concept of cell permeability, the lipid membrane that surrounds the cell favours the passage of only lipid soluble materials due to which liposolubility is an important factor that controls antimicrobial activity. On chelation, the polarity of the metal ion is reduced to a greater extent due to the overlap of the ligand, orbital and partial sharing of the positive charge of the metal ion with donor groups. Further, it increases the delocalisation of π-electrons over the whole chelate ring and enhances the lipophilicity of the complex. This increased lipophilicity enhances the penetration of the complexes into lipid membranes and blocking of metal binding sites on the enzymes of the microorganism. Among the various compounds tested, only the complex **5** is very active against all the bacteria. Complexes **6** and **7** show higher potential against the bacteria *E. coli* while the complexes **3**, **6** and **8** exhibited better activity against of *V. cholerae*. Eventhough the complexes possess higher activity than the free ligands, they could not reach the effectiveness of standard drug *Streptomycin*.

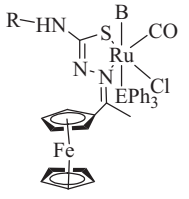

Fig. 9. General structure of new Ru(II) complexes (R = H, C_6H_5 or CH_3; E = P or As; B = PPh_3, $AsPh_3$, py or pip).

4. Conclusion

New hetero-binuclear complexes have been synthesized and characterized by the analytical and spectral methods. Though number of attempt made to get single crystals for X-ray diffraction studies were unsuccessful and the structure of the complexes has been confirmed by EXAFS. The electrochemical properties of the complexes have been examined and the higher comproportionation constant values suggesting that the current system can be a good molecular wire with very strong coupling between the metal centers and may be the first hetero metallic system exhibiting such a behaviour. The complexes also exhibited significant activity against the pathogenic bacteria such as *E. coli*, *V. cholerae* and *P. aeruginosa*. The complex **5** exhibited higher activity over all the bacteria which were taken. All the complexes exhibited higher activity than the free ligands.

Acknowledgement

Financial support received from Department of Science and Technology by SERC, New Delhi, India is gratefully acknowledged.

References

[1] H. Sasai, T. Arai, S. Watanabe, M. Shibasaki, Catal. Today 62 (2000) 17.
[2] T. Shribman, S. Kurz, U. Senff, F. Lindberg, E. Hey-Hawkins, M.S. Eisen, J. Mol. Catal. A: Chem. 129 (1998) 191.
[3] E.V. Marques, W.F. Ribeiro, C.A.L. Filgueiras, A. Abras, Hyperfine Interact. 96 (1995) 259.
[4] J.E.J.C. Graudo, N.L. Speziali, A. Abras, M. Horner, C.A.L. Filgueiras, Polyhedron 18 (1999) 2483.
[5] N. Yunyin, C. Peikun, Z. Hongyun, W. Qingan, L. Feng, Synth. React. Inorg. Met. Org. Chem. 28 (1998) 637.

[6] V. Weinmayr, Naturwissenschaften 45 (1958) 311.
[7] M. Rosenblum, Chemistry of the Iron Group Mettalocenes, Ferrocene, Ruthenocene, Osmocene. Part 1, Wiley, New York, 1975.
[8] A.N. Nesmeyanor, N.S. Kotchetkova, Russ. Chem. Rev. 43 (1974) 710.
[9] A.S. Tompa, Thermochim. Acta 77 (1984) 133.
[10] S.E. Sherman, S.J. Lippard, Chem. Rev. 87 (1987) 1153.
[11] K.P. Maier, H. Kopf, E.W. Neuse, J. Cancer Res. Clin. Oncol. 108 (1984) 336.
[12] E.Z. Neuse, F. Kanzawa, Appl. Organomet. Chem. 4 (1990) 19.
[13] K. Butler, US Patent No. 3382266 (1968).
[14] H.G. Petering, H.H. Buskirk, G.E. Underwood, Cancer Res. 64 (1964) 367.
[15] C.W. Johnson, J.W. Joyner, R.P. Perry, Antibiot. Chemother. 2 (1952) 636.
[16] J.P. Scovill, D.C. Kalyman, C.E. Farnchino, J. Med. Chem. 25 (1982) 1261.
[17] D. Kovala-Demertzi, P.N. Yadav, M.A. Demertzis, M. Coluccia, J. Inorg. Biochem. 78 (2000) 347.
[18] R. Karvembu, K. Natarajan, Polyhedron 21 (2002) 1721.
[19] R. Karvembu, K. Natarajan, Polyhedron 21 (2002) 219.
[20] A.I. Vogel, Textbook of Practical Oraganic Chemistry, 5th ed., Longman, London, 1989.
[21] B.S. Garg, L. Kapur, Inorg. Chim. Acta 170 (1990) 177.
[22] B.S. Garg, L. Kapur, Inorg. Chim. Acta 173 (1990) 223.
[23] Z. Xiaoxian, L. Yongmin, N. Fajun, N. Yongxiang, Polyhedron 11 (1990) 447.
[24] N. Ahmed, J.J. Levision, S.D. Robinson, M.F. Uttley, Inorg. Synth. 15 (1974) 48.
[25] S. Gopinathan, I.R. Unny, S.S. Deshpe, C. Gopinathan, Indian J. Chem. 25A (1986) 1015.
[26] A.W. Bauer, W.M. Kirby, J.C. Sherris, M. Turck, Am. J. Clin. Pathol. 45 (1966) 493.
[27] R. Prabhakaran, A. Geetha, M. Thilagavathi, R. Karvembu, V. Krishnan, H. Bertagnolli, K. Natarajan, J. Inorg. Biochem. 98 (2004) 2131.
[28] S. Gopinathan, S.S. Deshpande, C. Gopinathan, Indian J. Chem. 25A (1988) 126.
[29] R. Prabhakaran, R. Huang, K. Natarajan, Inorg. Chim. Acta 359 (2006) 3359, reference cited therein.
[30] R. Karvembu, S. Hemalatha, R. Prabhakaran, K. Natarajan, Inorg. Chem. Commun. 6 (2003) 486.
[31] R. Prabhakaran, S.V. Renukadevi, R. Karvembu, R. Huang, J. Mautz, G. Huttner, G. Subashkumar, K. Natarajan, Eur. J. Med. Chem. 43 (2008) 268.
[32] R. Prabhakaran, P. Kalaivani, R. Jayakumar, M. Zeller, A.D. Hunter, S.V. Renukadevi, E. Ramachandran, K. Natarajan, Metallomics, doi:10.1039/c0mt00062k.
[33] K.P. Deepa, K.K. Aravindakshan, Synth. React. Inorg. Met. Org. Chem. 30 (2000) 1601.
[34] A.B.P. Lever, Inorganic Electronic Spectroscopy, Elsevier, New York, 1984.
[35] K. Natarajan, U. Agarwala, Inorg. Nucl. Chem. Lett. 14 (1978) 7.
[36] R. Prabhakaran, R. Huang, S.V. Renukadevi, R. Karvembu, M. Zeller, K. Natarajan, Inorg. Chim. Acta 361 (2008) 2547.
[37] Y.C. Shi, H.M. Yang, W.B. Shen, C.G. Yan, X.Y. Hu, Polyhedron 23 (2004) 15.
[38] G. Muthusamy, N. Jayakumar, B. Manonmani, R. Shantha, K. Natarajan, Synth. React. Inorg. Met. Org. Chem. 22 (1992) 171.
[39] Y. Hoshino, Plat. Met. Rev 45 (2001) 2, reference cited therein.
[40] K. Moller, A. Borronwattananont, T. Beln, J. Phys. Chem. 93 (1989) 4562.
[41] G.C. Shen, A.M. Liu, M. Ichikawa, J. Chem. Soc., Faraday Trans 94 (1998) 1362.
[42] J.F. Bickley, A.A. La Penser, S.J. Higgins, C.A. Stuart, J. Chem. Soc. Dalton Trans. (2003) 4663.
[43] W.L. Man, T.M. Tang, T.W. Wong, T.C. Lau, S.M. Peng, W.T. Wong, J. Am. Chem. Soc. 126 (2004) 478.
[44] R. Prabhakaran, V. Krishnan, K. Pasumpon, D. Sukanya, E. Wendel, C. Jayabalakrishnan, H. Bertagnolli, K. Natarajan, Appl. Organomet. Chem. 20 (2006) 203.
[45] N.J. Holmes, A.R.J. Genge, W. Levason, M. Webster, J. Chem. Soc. Dalton Trans. (1997) 2331.
[46] B.G. Tweedy, Phytopathology 25 (1964) 910.